Efficient electrocatalytic water oxidation by nickel complexes: The effect of coordination number and ligand backbone structure on catalytic properties

Jinlin Hu[a], Zhichao Qi[a], Lianghui Zhang[a], Xiangming Liang[b], Junqi Lin[a,*], Zhijun Ruan[a,*], Shanshan Liu[a,*]

[a] Hubei Key Laboratory of Processing and Application of Catalytic Materials, College of Chemistry and Chemical Engineering, Huanggang Normal University, Huanggang, 438000 China.

[b] School of Basic Medical Sciences, Ningxia Medical University, Yinchuan, 750004, China.

Email: linjunqi@hgnu.edu.cn, ruanzhijun87@126.com, liushanshanlhl@163.com

Table S1 Crystallographic data and processing parameters for complex **1**

Complex parameters	$[Ni(MePy_2tacn)(H_2O](ClO_4)_2 \cdot H_2O$ (**1**·H_2O)
Empirical formula	$C_{19}H_{31}Cl_2N_5NiO_{10}$
Formula weight	619.10
Temperature / K	296.00
Wavelength / Å	0.71073
Crystal system	monoclinic
Space group	$P2_1/c$
a / Å	17.933(3)
b / Å	8.9773(17)
c / Å	17.496(4)
α / deg	90
β / deg	112.996(6)
γ / deg	90
Volume / Å^3	2592.8(8)
Z	4
Calculated density / Mg m^3	1.586
Absorption coefficient	1.016 mm^{-1}
F(000)	1288
Crystal size / mm	0.29 × 0.26 × 0.23
2*θ* range / deg	3.081 to 26.442
Index ranges	-22<=h<=22, -11<=k<=11, -21<=k<=21
Reflections collected	54306
Independent reflections	5279 [R_{int} = 0.1065]
Completeness to theta = 24.792°	98.6 %
Absorption correction	Semi-empirical from equivalents
Refinement method	Full-matrix least-squares on F^2
Data / restraints / parameters	5279 / 0 / 339
Goodness-of-fit on F^2	1.039
Final R indices [I>2sigma(I)]	R_1 = 0.0490, wR_2 = 0.1272
R indices (all data)	R_1 = 0.0657, wR_2 = 0.1407
Largest diff. peak and hole	0.780 and -0.374 e.Å^{-3}

$R_1 = \Sigma||F_o| - |F_c||/\Sigma|F_o|$, $wR_2 = [\Sigma(|F_o|^2 - |Fc|^2)^2/\Sigma(Fo_2)]^{1/2}$

Table S2 Crystallographic data and processing parameters for complex **2**

Complex parameters	$[Ni(Py_3tacn)](ClO_4)_2 \cdot CH_3CN$ (**2**·CH_3CN)
Empirical formula	$C_{26}H_{33}Cl_2N_7NiO_8$
Formula weight	701.193
Temperature / K	298.00
Wavelength / Å	0.71073
Crystal system	monoclinic
Space group	$P2_1/c$
a / Å	16.7337(6)
b / Å	14.1267(4)
c / Å	13.8407(5)
α / deg	90
β / deg	112.985(1)
γ / deg	90
Volume / Å^3	3012.07(18)
Z	4
Calculated density / Mg m^3	1.546
Absorption coefficient	0.882 mm^{-1}
F(000)	1459.6
Crystal size / mm	0.32 × 0.28 × 0.26
2*θ* range / deg	3.92 to 56.62
Index ranges	-22<=h<=22, -18<=k<=18, -18<=k<=18
Reflections collected	61263
Independent reflections	7399 [R_{int} = 0.1052]
Completeness to theta = 24.792°	99.5 %
Absorption correction	Semi-empirical from equivalents
Refinement method	Full-matrix least-squares on F^2
Data / restraints / parameters	7399 / 0 / 398
Goodness-of-fit on F^2	1.021
Final R indices [I>2sigma(I)]	R_1 = 0.0522, wR_2 = 0.1323
R indices (all data)	R_1 = 0.0751, wR_2 = 0.1519
Largest diff. peak and hole	0.85 and -0.53 e.Å^{-3}

$R_1 = \Sigma||F_o| - |F_c||/\Sigma|F_o|$, $wR_2 = [\Sigma(|F_o|^2 - |Fc|^2)^2/\Sigma(Fo_2)]^{1/2}$

Table S3 Selected bond lengths for complex **1** and **2**

Complex	**1**	Complex	**2**
Bond length (Å)		Bond length (Å)	
Ni1–N1	2.101(3)	Ni1–N1	2.105(2)
Ni1–N2	2.062(3)	Ni1–N2	2.096(2)
Ni1–N3	2.120(3)	Ni1–N3	2.105(2)
Ni1–N4	2.075(3)	Ni1–N4	2.065(2)
Ni1–N5	2.056(3)	Ni1–N5	2.087(2)
Ni1–O1	2.123(2)	Ni1–N6	2.072(2)

Table S4 Selected bond angles for complex **1** and **2**

Complex	**1**		**2**
Bond angles (deg)		Bond angles (deg)	
N1–Ni1–N2	80.57(10)	N1–Ni1–N2	84.10(9)
N1–Ni1–N3	164.16(11)	N1–Ni1–N3	83.91(10)
N1–Ni1–N4	96.35(11)	N1–Ni1–N4	98.14(10)
N1–Ni1–N5	96.68(10)	N1–Ni1–N5	80.34(10)
N1–Ni1–O1	86.11(10)	N1–Ni1–N6	164.74(9)
N2–Ni1–N3	83.76(11)	N2–Ni1–N3	84.09(9)
N2–Ni1–N4	85.62(11)	N2–Ni1–N4	164.79(10)
N2–Ni1–N5	166.56(11)	N2–Ni1–N5	97.49(9)
N2–Ni1–O1	99.59(11)	N2–Ni1–N6	81.00(9)
N3–Ni1–N4	84.74(11)	N3–Ni1–N4	81.21(10)
N3–Ni1–N5	99.11(11)	N3–Ni1–N5	163.90(10)
N3–Ni1–O1	94.23(11)	N3–Ni1–N6	97.73(9)
N4–Ni1–N5	81.60(11)	N4–Ni1–N5	97.72(10)
N4–Ni1–O1	174.55(11)	N4–Ni1–N6	97.09(9)
N5–Ni1–O1	93.31(10)	N5–Ni1–N6	98.35(10)

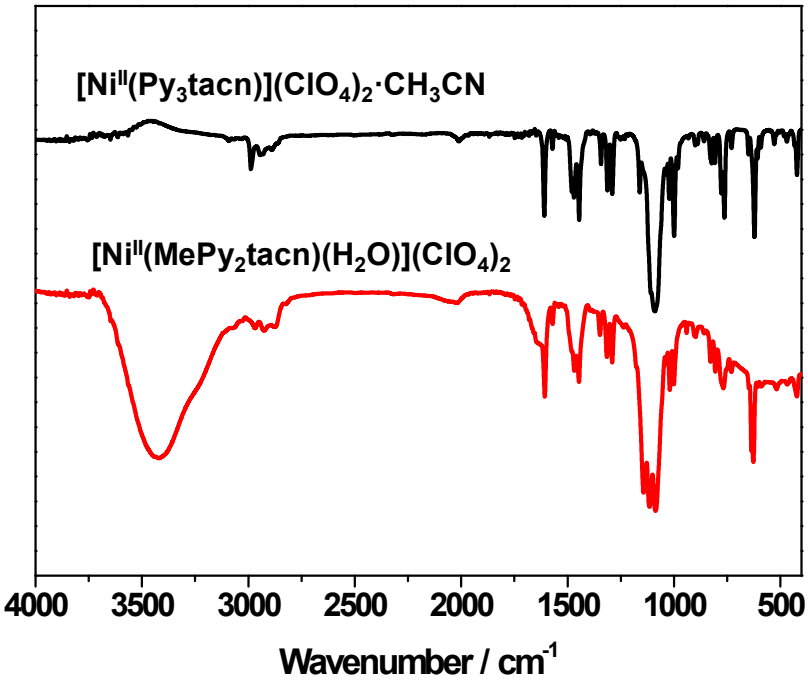

Fig. S1 The infrared spectra of complex **1** and **2**.

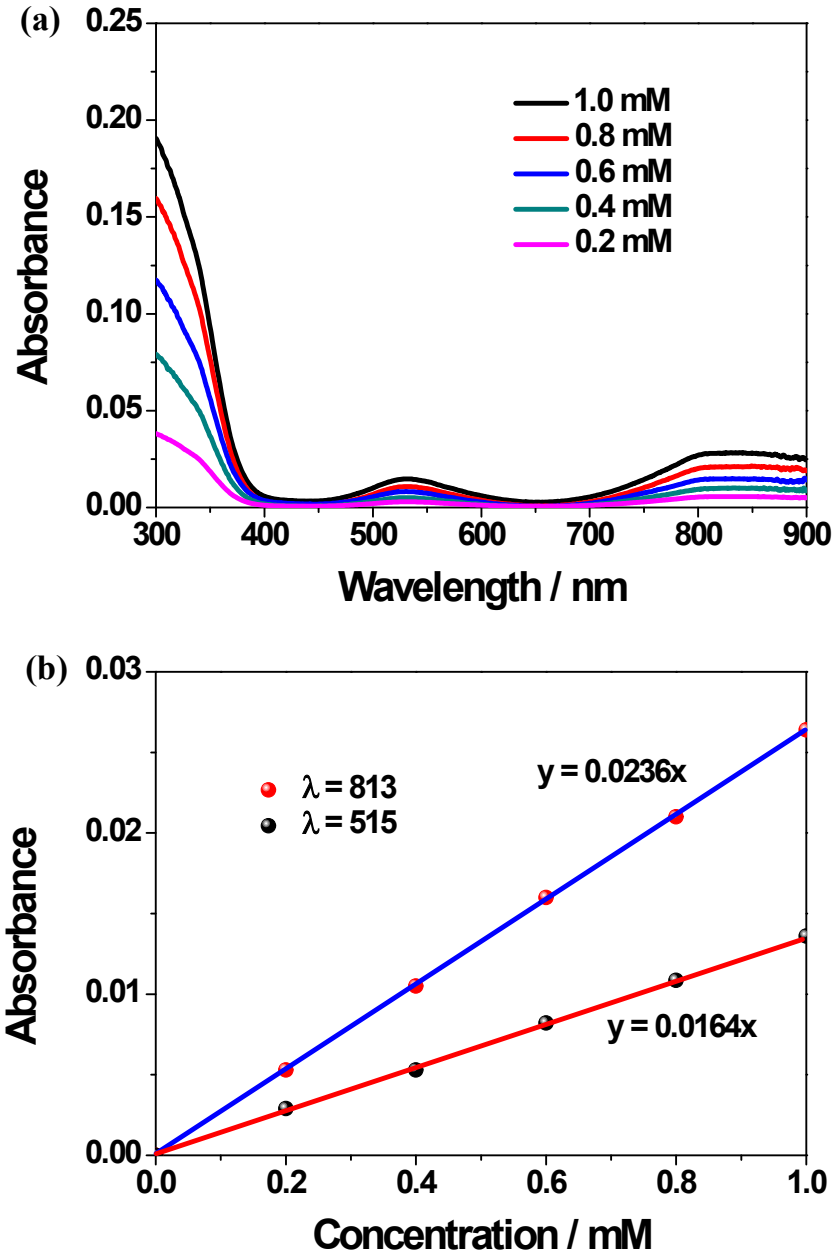

Fig. S2 (a) UV-vis absorption spectra of various concentration of **1** in 0.1 M acetate buffer solution (ABS) at pH 6.0. (b) Liner dependence of the absorbance value of **1** on its concentration.

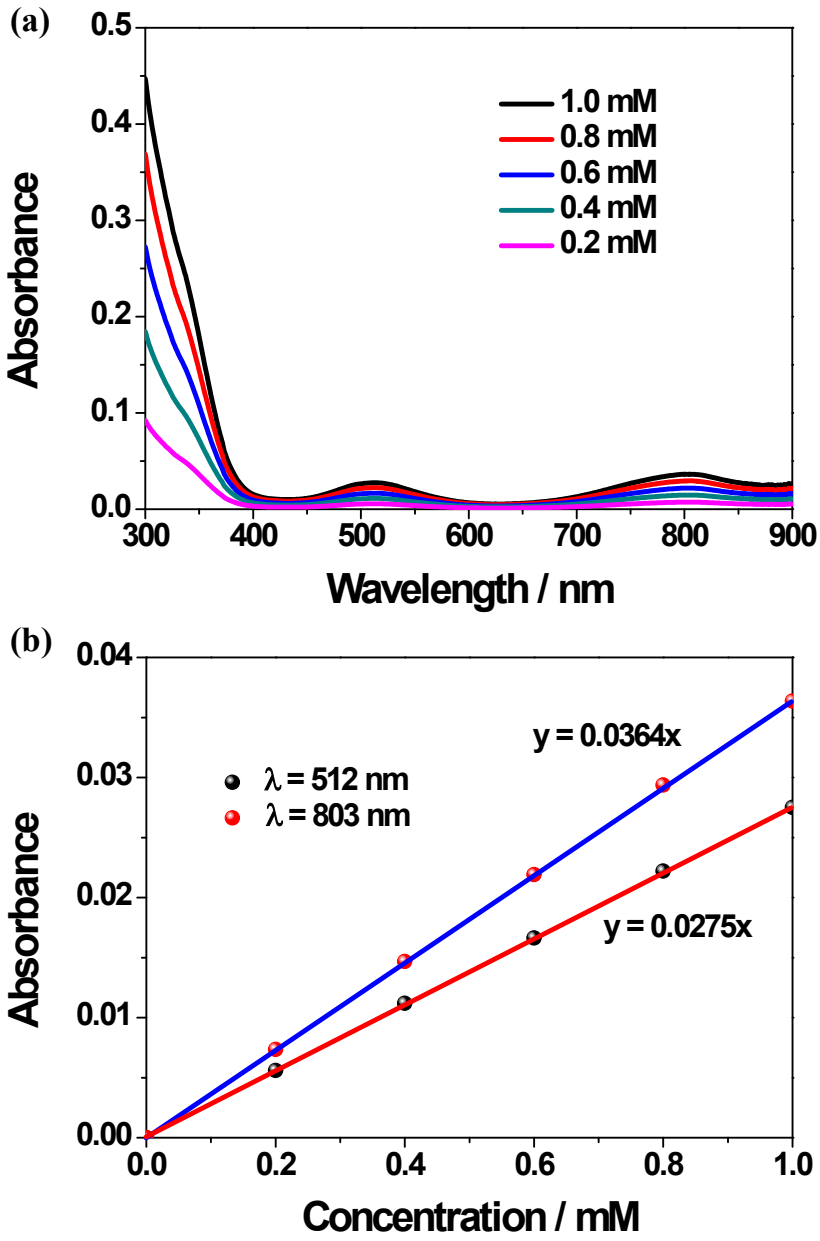

Fig. S3 (a) UV-vis absorption spectra of various concentration of **2** in 0.1 M ABS at pH 6.0. (b) Liner dependence of the absorbance value of **2** on its concentration.

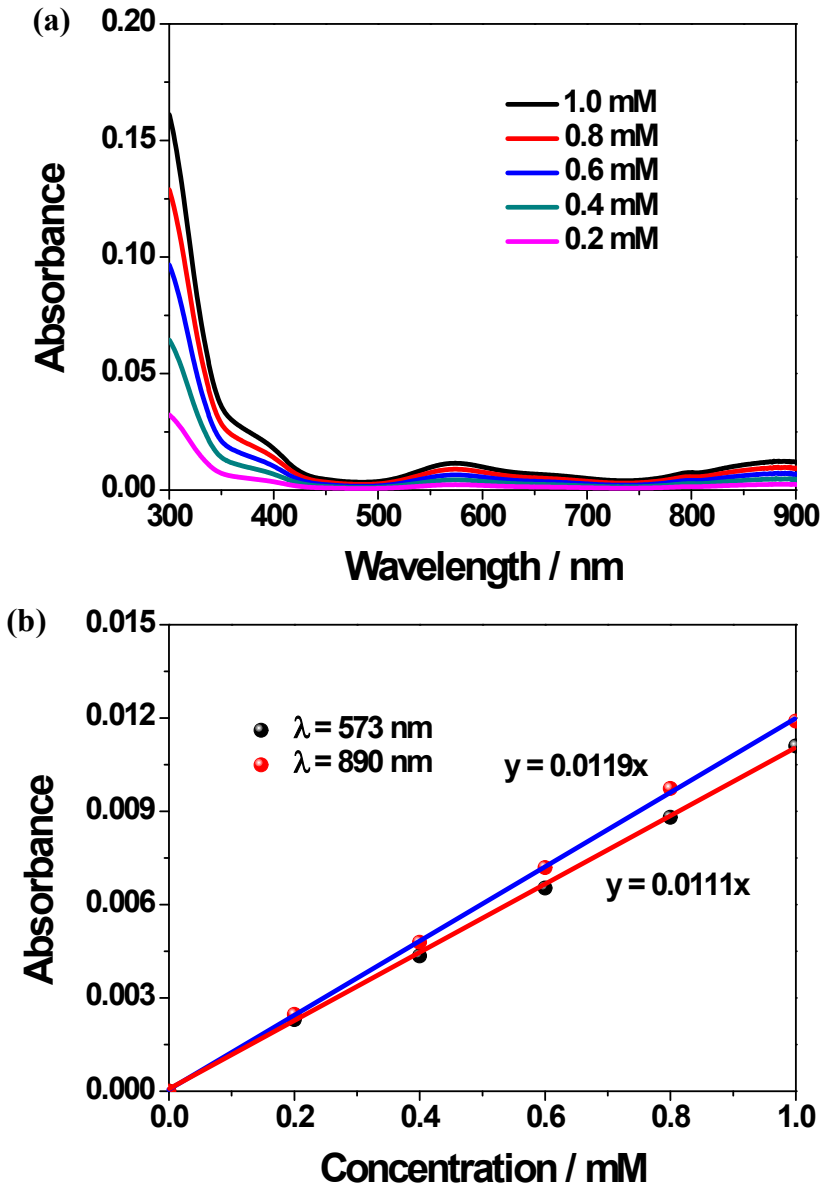

Fig. S4 (a) UV-vis absorption spectra of various concentration of **3** in 0.1 M ABS at pH 6.0. (b) Liner dependence of the absorbance value of **3** on its concentration.

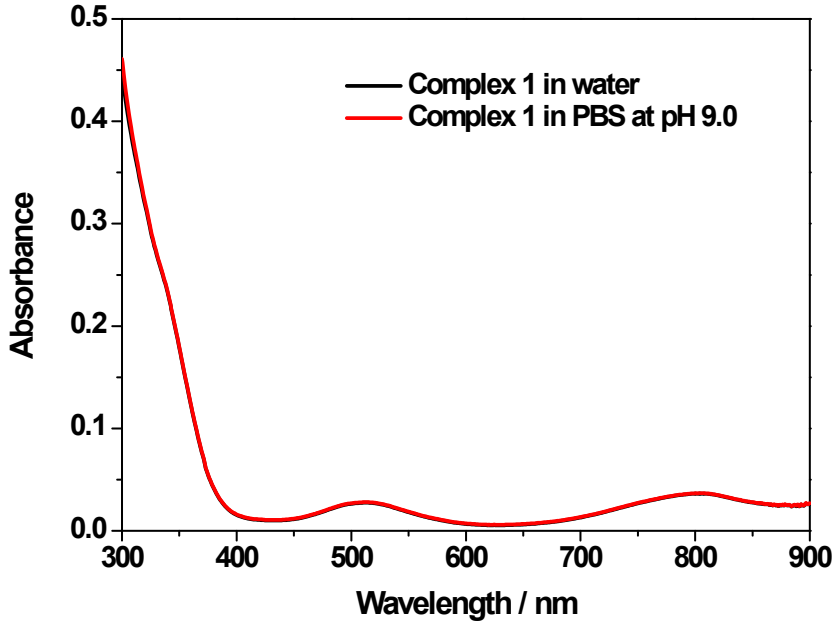

Fig. S5 UV-vis absorption of 1 mM of **2** in water and phosphate buffer solution (PBS) at pH 9.0). To ensure adequate pH buffering capacity, PBS was substituted for the ABS in the UV-Vis absorption tests of **1** under alkaline conditions. This difference in the buffer species does not affect the relevant conclusions.

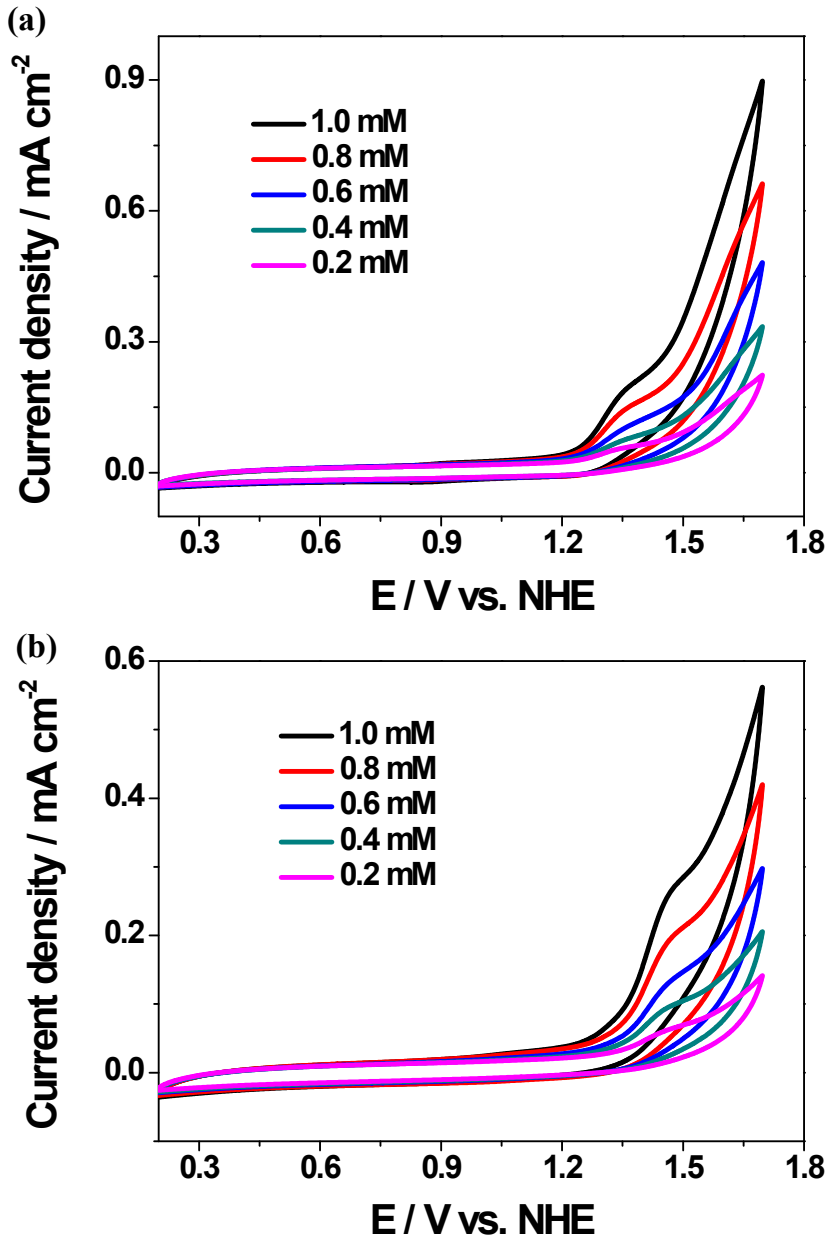

Fig. S6 (a) CV curve of 1 mM of **1** in 0.1 M ABS at pH 6.0 (b) CV curve of 1 mM of **2** in 0.1 M ABS at pH 6.0. Scan rate of 100 mV/s.

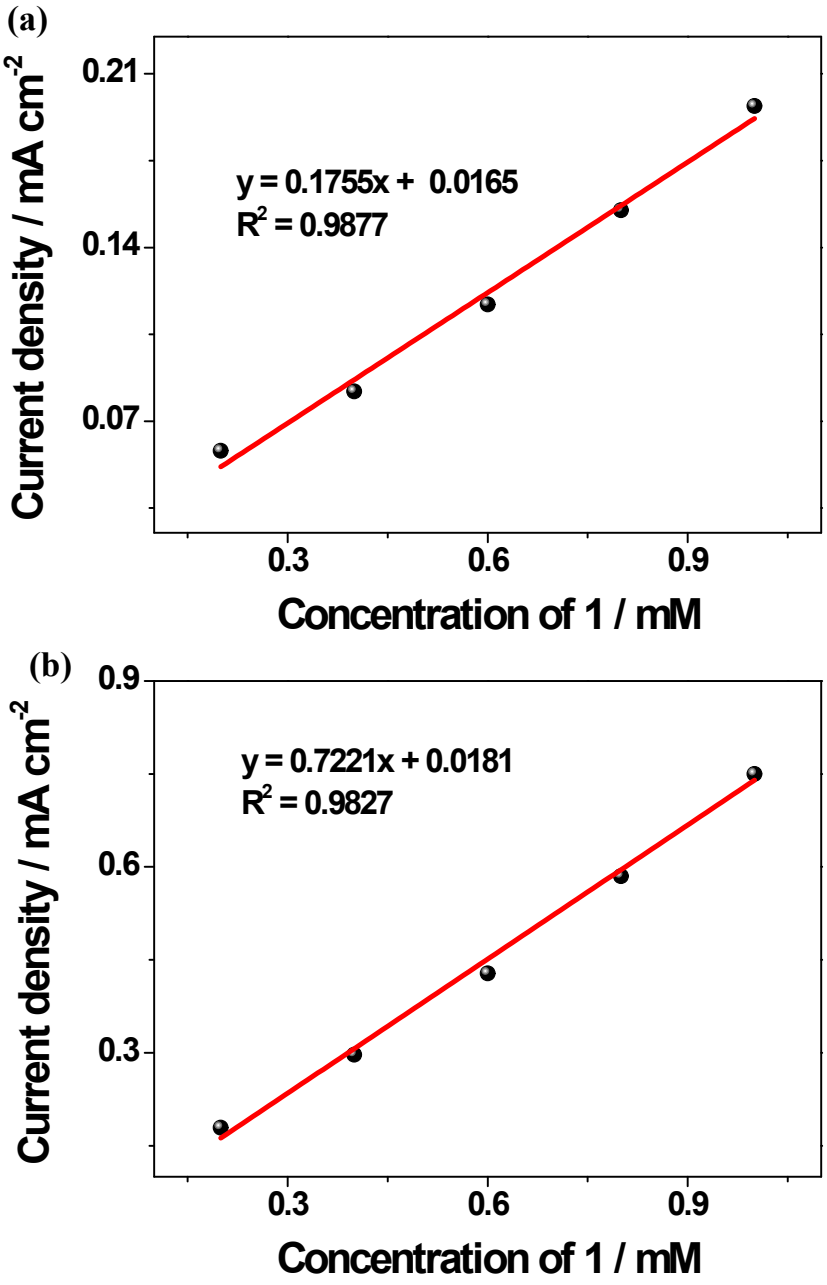

Fig. S7 (a) The dependence of the non-catalytic current density on the concentration of **1**. (b) the relationship between the catalytic current density and the concentration of **1**.

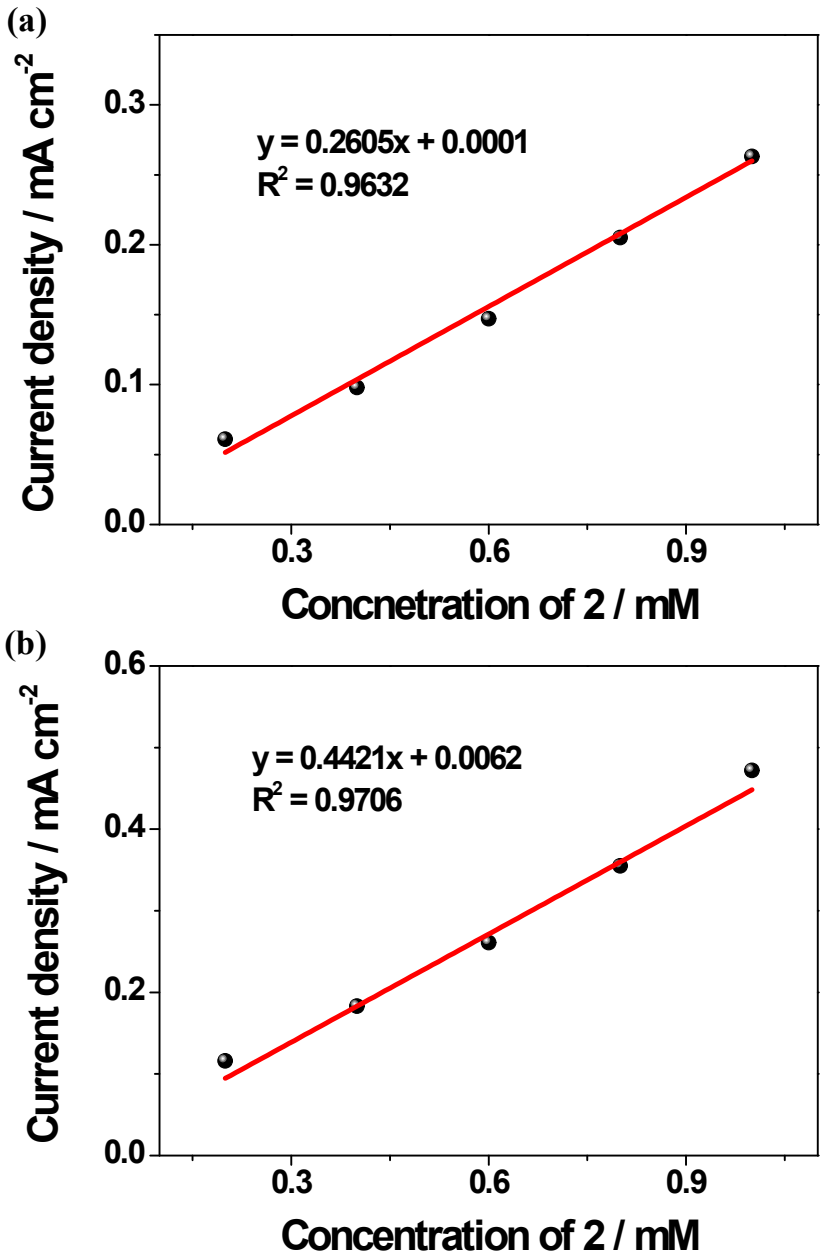

Fig. S8 (a) The dependence of the non-catalytic current density on the concentration of **2**. (b) the relationship between the catalytic current density and the concentration of **2**.

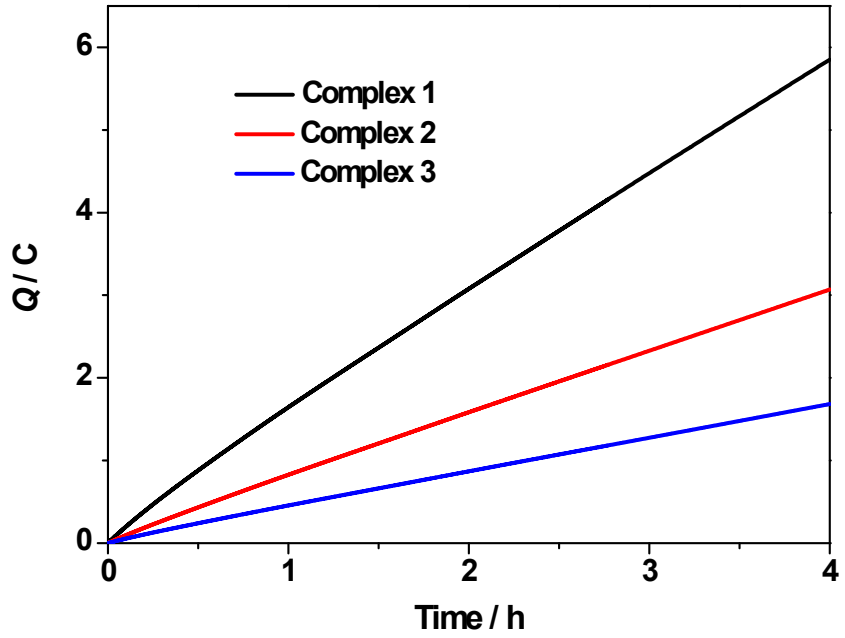

Fig. S9 Chronocoulometric plots from CPE with 1 mM of **1**–**3** at an applied potential of 1.65 V vs. NHE.

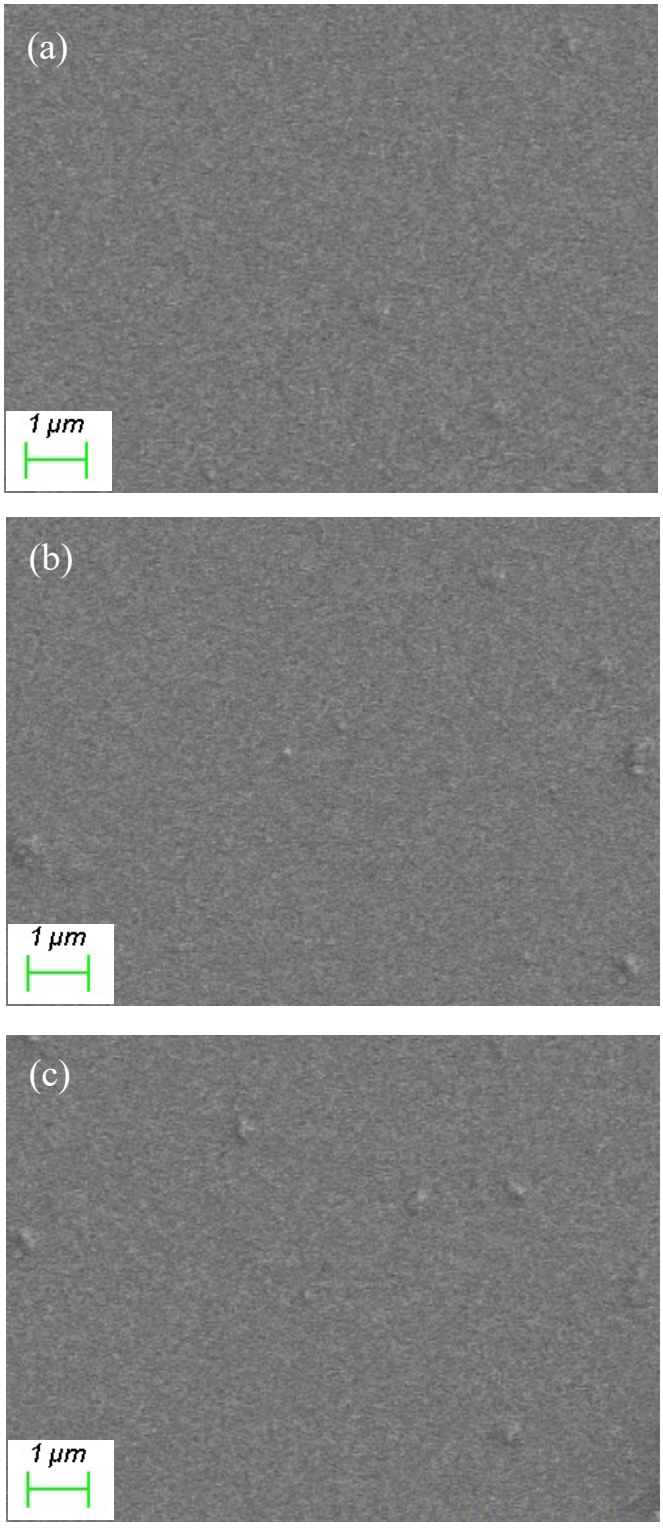

Fig. S10 Morphology of clean ITO electrode (a), as-used ITO-**1** (b) and as-used ITO-**2** (c).

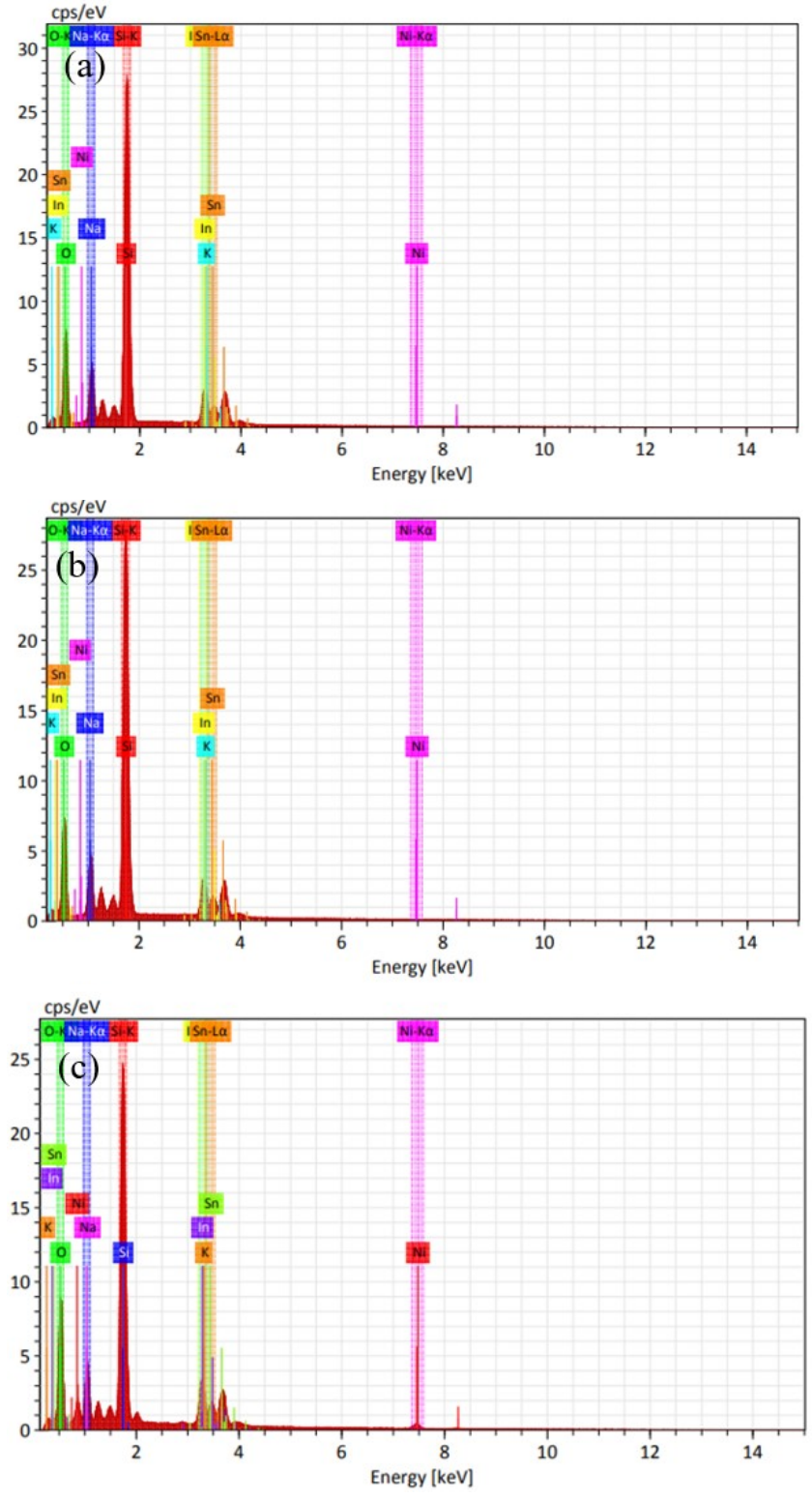

Fig. S11 EDS analysis on the surface of clean ITO electrode (a), as-used ITO-**1** (b) and as-used ITO-**2** (c).

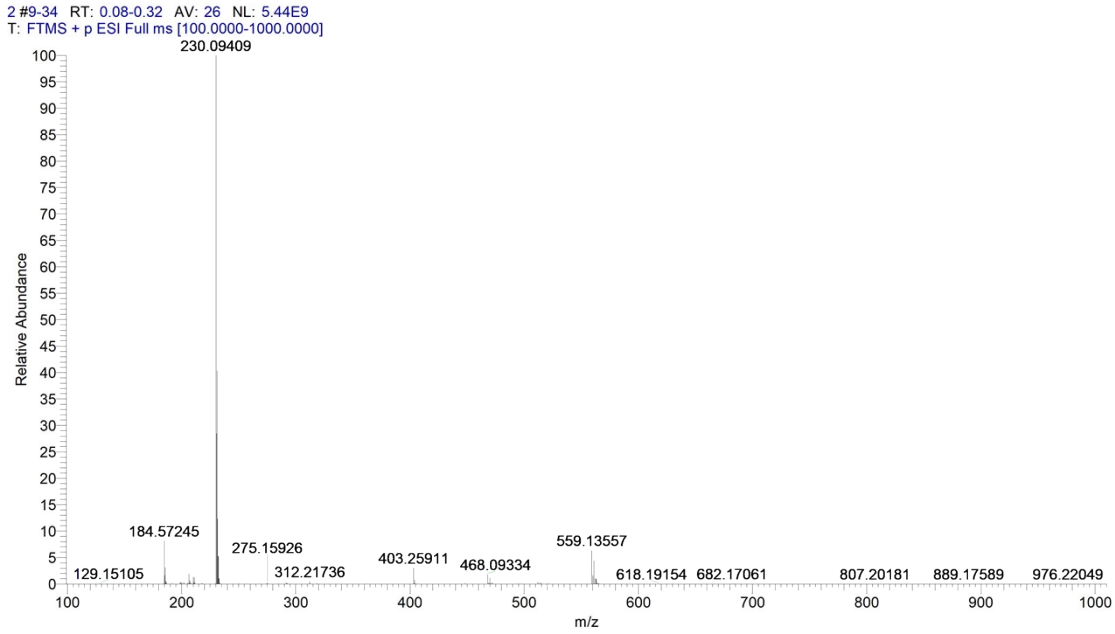

Fig. S12 High resolution mass spectrometry of complex **1** after the CPE test.

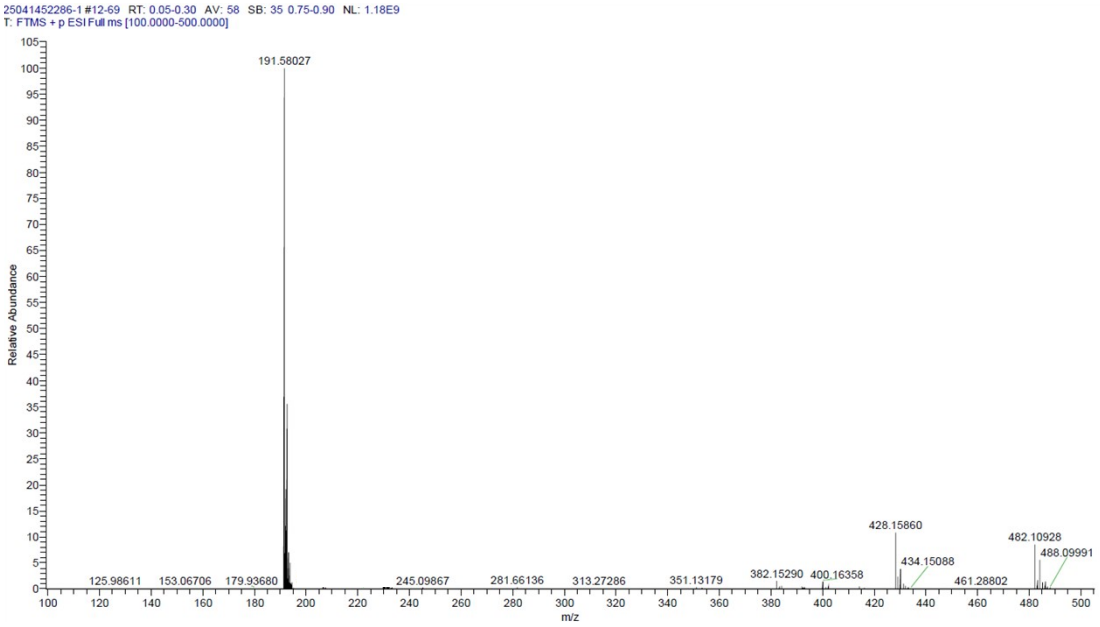

Fig. S13 High resolution mass spectrometry of complex **2** after the CPE test.

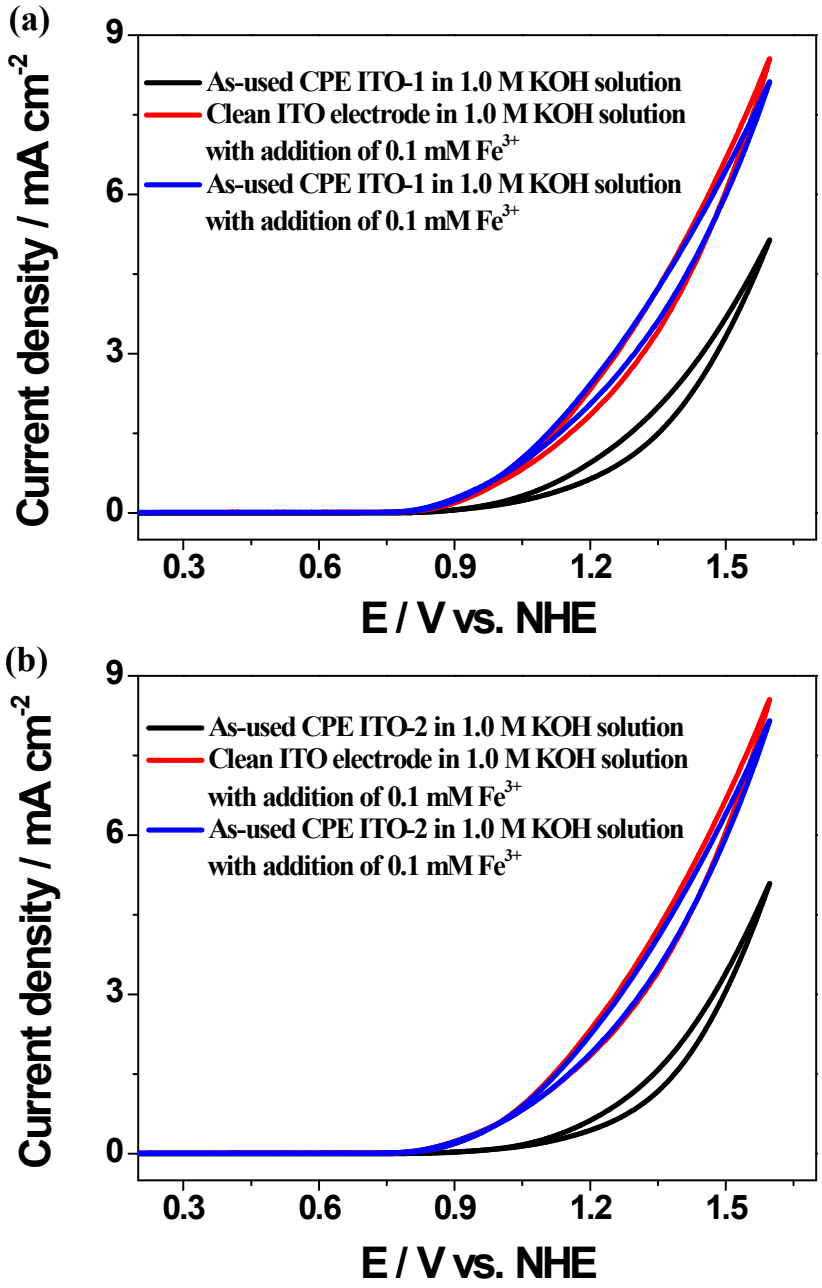

Fig. S14 CV test of as-used CPE test ITO electrode of **1** (a) and **2** (b) in 1.0 M KOH solution, clean ITO electrode in 1.0 M KOH solution with addition of 0.1 mM Fe^{3+} and as-used ITO electrode of **1** (a) and **2** (b) in 1.0 M KOH solution with addition of 0.1 mM Fe^{3+}.

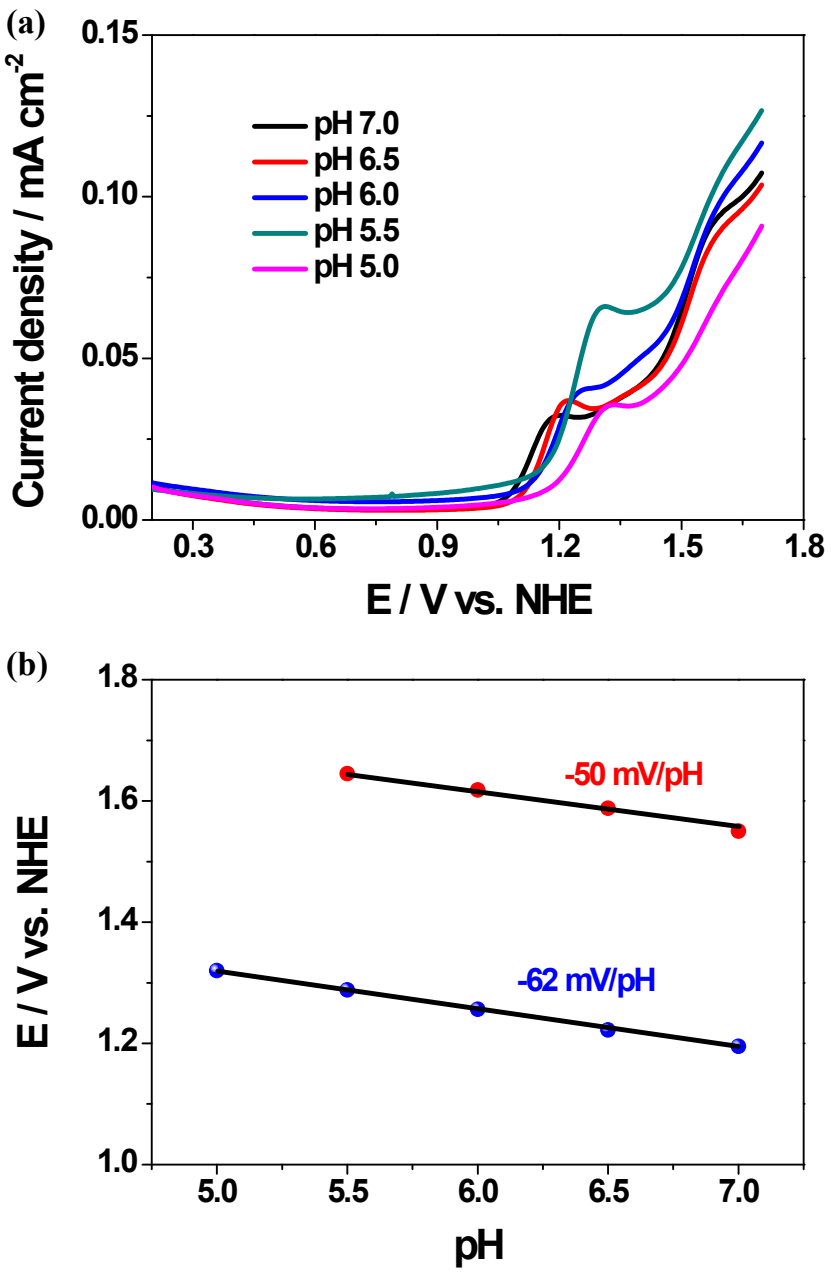

Fig. S15 (a) DPV test of 1 mM of **1** in 0.1 M ABS at various pH values. (b) the relationship between the potential of each redox couple of **1** and the pH value.

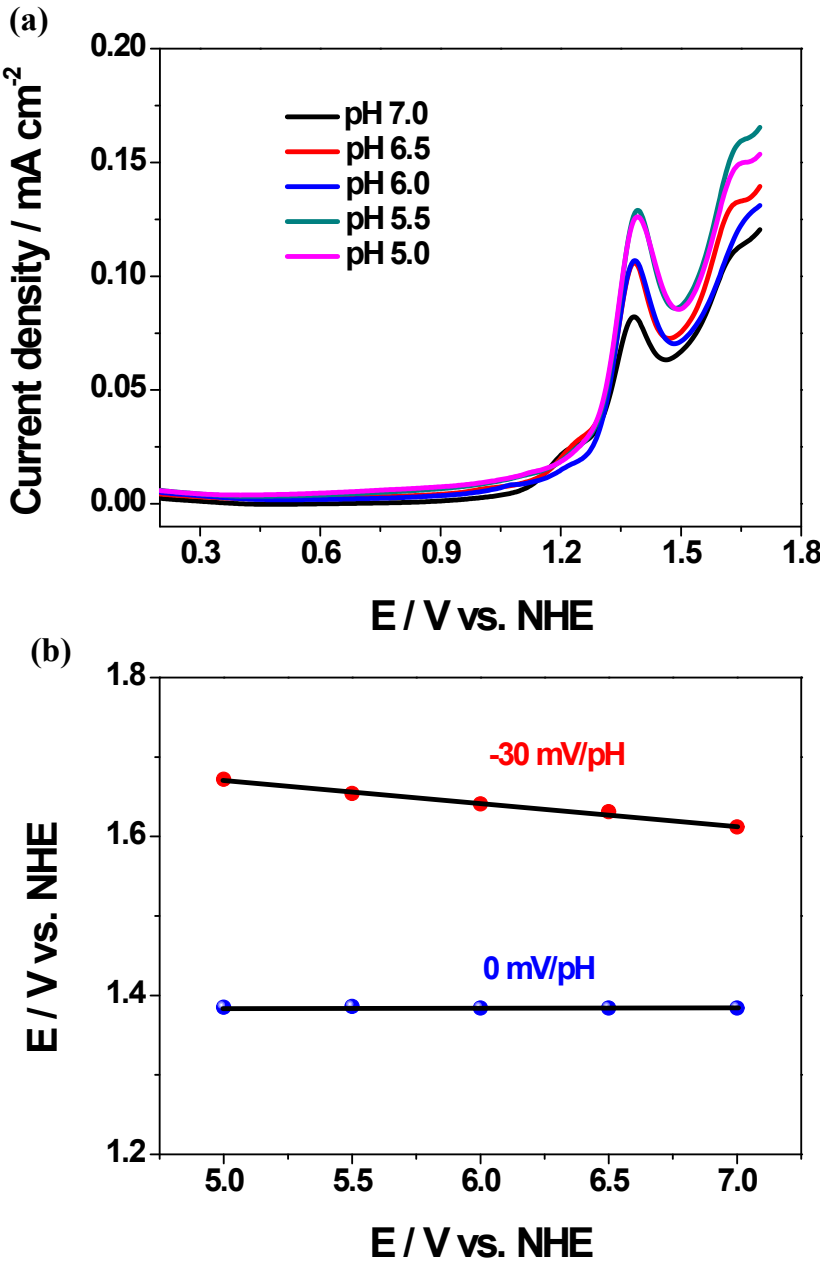

Fig. S16 (a) DPV test of 1 mM of **2** n 0.1 M ABS at various pH values. (b) the relationship between the potential of each redox couple of **2** and the pH value.

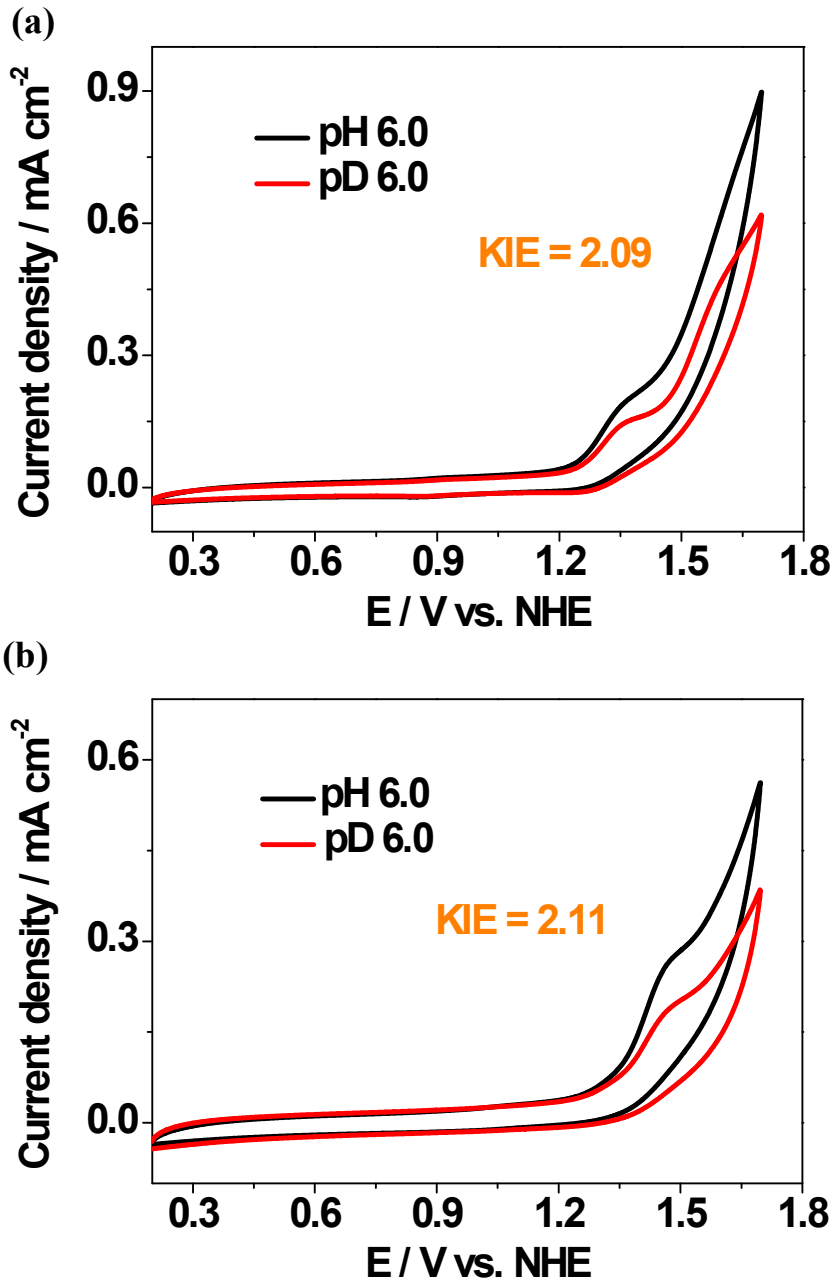

Fig. S17 Stabilized CV of 1 mM of **1** (a) and **2** (b) in H_2O ABS at pH 6.0 and D_2O ABS at pD 6.0 with a glassy carbon working electrode at a scan rate of 100 mV s^{-1}.

Table S5 Onset overpotential of **1**, **2** and some previously reported molecular WOC based on Ni complex

Catalyst [a]	pH	η/mV [b]	Ref.
$[Ni(L)(H_2O)_2]^{2+}$	6.5	533	S1
$[Ni^{II}\text{-}L1]^{2+}$	7.0	580	S2
$[Ni(TAML)]^{2-}$	7.0	680	S3
$[Ni(tmbptn)(H_2O)]^{2+}$	9.0	581	S4
$[NiL]^{2+}$	9.0	550	S5
Ni-PY5	10.8	800	S6
$[Ni(MePy_2tacn)(H_2O)](ClO_4)_2$	6.0	510	This work
$[Ni(Py_3tacn)](ClO_4)_2$	6.0	610	This work

[a] Structures of the catalysts are listed as below.

[b] η = Onset overpotential

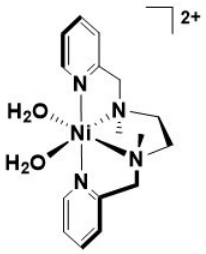

$[Ni(L)(H_2O)_2]^{2+}$

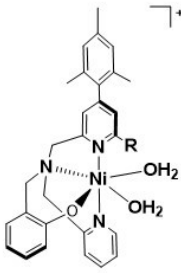

$[Ni^{II}\text{-}L1]^{2+}$

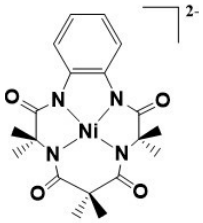

$[Ni(TAML)]^{2-}$

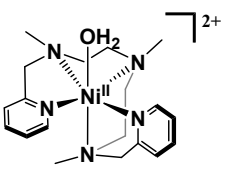

$[Ni(tmbptn)(H_2O)]^{2+}$

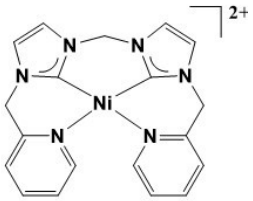

$[NiL]^{2+}$

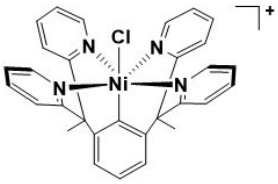

Ni-PY5

Notes and references

1 G.-Y. Luo, H.-H. Huang, J.-W. Wang and T.-B. L, *ChemSusChem*, 2016, **9**, 485–491.

2 D. Wang and C. O. Bruner, *Inorg. Chem.*, 2017, **56**, 13638–13641.

3 H. Lee, X. Wu and L. Sun, *ChemSusChem*, 2020, **13**, 3277–3282.

4 X. Chen, X. Liao, C. Dai, L. Zhu, L. Hong, X. Yang, Z. Ruan, X. Liang and J. Lin, *Dalton Trans*., 2022, **51**, 18678–18684.

5 H. M. Shahadat, H. A. Younus, N. Ahmad, M. A. Rahaman., Z. A. K. Khattak, S. Zhuiykov and F. Verpoort, *Catal. Sci. Technol*., 2019, **9**, 5651–5659.

6 L. Wang, L. Duan, R. B. Ambre, Q. Daniel, H. Chen, J. Sun, B. Das, A. Thapper, J. Uhlig, P. Dinér and L. Sun, *J. Catal*., 2016, **335**, 72–78.